Pathological Pattern Formation in Absence Epilepsy: A Theoretical Framework to Unify Global and Focal Aspects

Dong-Ping Yang[1,2,*] and P. A. Robinson[1,2]

[1] *School of Physics, University of Sydney, New South Wales 2006, Australia*
[2] *Center for Integrative Brain Function, University of Sydney, New South Wales 2006, Australia*

(Dated: June 5, 2018)

Absence epilepsy is characterized by a sudden paroxysmal loss of consciousness accompanied by oscillations of activity propagating over many brain areas. Although the primary generalized absence seizures are traditionally underlain by the global corticothalamic system, converging experimental evidence supports the focal theory of absence epilepsy. Here a theory is proposed to unify both global and focal aspects of absence epilepsy in a physiology-based corticothalamic model with spatial heterogeneity representing an initial seizure focus, emphasizing the effect of local cortical connectivity and cortical propagation. Numerical simulations and analytical calculations are combined to investigate the emergent spatiotemporal dynamics induced by the seizure focus as well as their underlying dynamical mechanisms. The results categorize the spatiotemporal dynamics into three scenarios: seizure suppression, seizure localization and seizure generalization, where robust self-organized waves agree well with experimental wave rhythms and spatial extensions during seizures for global and focal aspects, respectively. Our findings provide a biophysical and mechanistic explanation of higher frequency and amplitude of the waves observed in genetic rat models with absence epilepsy, and imply that global and focal absence epilepsy could be unified in the framework of pathological pattern formation. Predictions are also presented for future experimental tests.

I. INTRODUCTION

Absence epilepsy is an idiopathic nonconvulsive generalized epilepsy, consisting with a sudden paroxysmal loss of consciousness accompanied by abnormal brain oscillatory activity: 2.5–4 Hz 'spike-and-wave' discharges (SWDs) in electroencephalogram (EEG) and electrocorticogram (ECoG) [1]. These oscillations propagate rapidly over many brain areas and reflect the macroscopic dynamical properties of neuronal populations. Many experimental results led to the corticothalamic theory that the interactions between cortex and thalamus generate absence seizures [2–7]. However, there was recently converging evidence in animal models [8–11] showing that absence seizures can be triggered from a specific cortical focus, leading to a focal theory of absence epilepsy [12]. Also, an accurate source analysis from dense-array surface electrodes led to the suggestion that absence seizures in human patients were not truly 'generalized', with immediate and global cortical involvement, but rather were initiated, then propagated, from specific cortical regions [13]. It remains unclear how both global and local aspects of absence seizures are related [6, 14, 15].

Absence epilepsy in humans was well established in two genetic rat models: the Wistar Albino Glaxo/Rijswijk (WAG/Rij) and Genetic Absence Epilepsy Rats from Strasbourg (GAERS), with validity demonstrated by phenomenological similarities and performance prediction based on pharmacological data [16]. One of main arguments is the frequency difference of SWDs: 7–11 Hz in rats [8, 10] and 2.5–4 Hz in humans or cats [1, 15]. Although there are no *a priori* reasons why the SWD frequency must be the same in all species, to our best knowledge, it is still unknown how a spontaneous 7–11 Hz rhythm can be initiated and sustained in the cortical focus via the so-called somatosensory-thalamo-cortical network or the cortical propagation [8, 10, 15]. Actually, the cortex and the thalamus form one complex oscillatory network, providing a resonant circuit to amplify and sustain the SWDs, with the resonance considered as an emerging property of the corticothalamic system [7]. So the higher SWD frequency in rats may be accounted for by different brain sizes and axon properties; e.g., delay time, propagation speeds as well as interaction strengths between neuronal populations.

However, there is another significant difference of absence seizures between rats and humans: *spatial extension*. In rats, higher frequency and amplitude SWDs were generated with a cortical 'focus' found within the perioral sub-region of the somatosensory cortex [8]. During spontaneous absence seizures, the cortical focus drives widespread corticothalamic networks, which are responsible for the immediate onset, widespread generalization and high synchrony of SWDs. Specifically, the simultaneous recorded field potentials have a decreasing amplitude along the propagation on cortex [8], and thus are more spatially localized. On the other hand, in humans, SWDs activity is more generalized over the whole brain [13]. It is also commonly in the experimental findings that the low-frequency rhythms are much more generalized in space, whereas the higher frequency oscillations are localized to restricted cortical areas [17, 18]. So we are here to investigate the effect of spatial extensions on the observed oscillating rhythms, and to ask whether there is a theoretical framework accounting for both global and focal aspects of absence epilepsy and what is the under-

* dp.yang@sydney.edu.au

lying dynamical mechanism.

This paper explores how the focal seizure can generalize and proposes the hypothesis that both global and focal absence seizures could be unified in the theoretical framework of pathological pattern formation induced by an initial seizure focus [19, 20]. Specifically, we hypothesize that the focal absence seizure is an electro-clinical symptom associated with seizure localization: an abnormal state with seizure activity spatially localized, while the global absence seizure is associated with seizure generalization: seizure activity propagating outwards from seizure focus over the whole system. We investigate this hypothesis theoretically using a physiologically based model with spatial heterogeneity to explore spatiotemporal dynamics of the coupled cortex and thalamus. We analyze the conditions for an initial seizure focus to be suppressed, localized, or to generalize the activity that spreads over the whole brain, and explore the roles of local cortical connectivity and cortical propagation. We find that the emergent spatiotemporal dynamics induced by the seizure focus can unify both global and focal aspects of absence epilepsy, and the self-organized cortical waves have robust rhythms, and the wave rhythms and spatial extensions are comparable with experimental observations. The underlying dynamical mechanisms are discovered by employing eigenvalue spectra and corresponding eigenmodes at critical states. We conclude with some experimentally testable predictions.

II. MATERIALS & METHODS

The corticothalamic model is described in Sec. II A, following previous work [21]. Then we introduce an initial seizure focus in the corticothalamic model with 2D spatial heterogeneity in Sec. II B. The simulation method is described in Sec. II C. Afterwards, we present the analytical calculation of steady states and their linear stability analysis in Sec. II D.

A. Corticothalamic model

The corticothalamic system can be described by a continuum approach at the macroscopic level. Large-scale neural activity arises from interactions between several neural populations, notably excitatory and inhibitory cortical neurons and specific subcortical nuclei such as thalamus. In such a model [21], the variables represent local mean values at position $\boldsymbol{r} = (r_x, r_y)$: the local mean cell-body potential V_a, the mean firing rate Q_a, and the propagating axonal field ϕ_a ($a = e, i, r, s$ for excitatory, inhibitory, reticular, and relay neurons, respectively). The logic of these collective state variables is summarized in Fig. 1(A).

Firstly, the firing rate Q_a is a sigmoid function of the

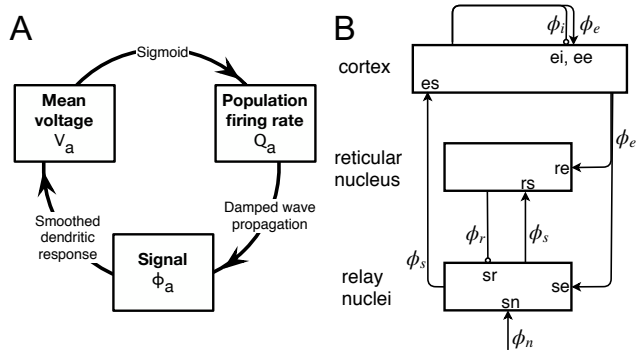

FIG. 1. The corticothalamic model. (A) The cycle of the system variables: V_a, Q_a and ϕ_a. (B) Schematic of the corticothalamic interactions, showing the locations ab at which couplings act.

potential V_a with

$$Q_a(\boldsymbol{r}, t) = S[V_a(\boldsymbol{r}, t)] \tag{1}$$

$$= \frac{Q_{\max}}{1 + \exp\{-[V_a(\boldsymbol{r}, t) - \theta']/\sigma'\}}, \tag{2}$$

where $Q_{\max}$ is the maximal firing rate, θ' is the mean firing threshold, and $\sigma'\pi/\sqrt{3}$ is its standard deviation.

Secondly, neuronal firing generates a field signal ϕ_a and sends it through the extended axons toward other populations approximately according to the damped wave equation [22, 23]

$$\left(D_a - r_a^2 \nabla^2\right) \phi_a(\boldsymbol{r}, t) = Q_a(\boldsymbol{r}, t), \tag{3}$$

with

$$D_a = \left(\frac{1}{\gamma_a}\frac{\partial}{\partial t} + 1\right)^2, \tag{4}$$

where $\gamma_a = v_a/r_a$ governs the damping of propagating waves, and $r_a \& v_a$ are the characteristic range and conduction velocity of axons extending from population a, respectively [23].

Finally, each population's potential V_a results when synaptic inputs from various types of afferent neurons are summed after being filtered and smeared out in time due to synaptic neurotransmitter, receptor dynamics and passage through the dendritic tree. So

$$D_\alpha V_e(\boldsymbol{r}, t) = \nu_{ee}\phi_e(\boldsymbol{r}, t) + \nu_{ei}\phi_i(\boldsymbol{r}, t) + \nu_{es}\phi_s(\boldsymbol{r}, t - t_d), \tag{5}$$

$$D_\alpha V_r(\boldsymbol{r}, t) = \nu_{re}\phi_e(\boldsymbol{r}, t - t_d) + \nu_{rs}\phi_s(\boldsymbol{r}, t), \tag{6}$$

$$D_\alpha V_s(\boldsymbol{r}, t) = \nu_{se}\phi_e(\boldsymbol{r}, t - t_d) + \nu_{sr}\phi_r(\boldsymbol{r}, t) + \nu_{sn}\phi_n(\boldsymbol{r}, t), \tag{7}$$

with the synaptodendritic filter operator

$$D_\alpha = \frac{1}{\alpha\beta}\frac{d^2}{dt^2} + \left(\frac{1}{\alpha} + \frac{1}{\beta}\right)\frac{d}{dt} + 1, \tag{8}$$

where α and β are the mean decay and rise rates of the soma response to an impulse arriving at a dendritic synapse [23].

Note that the input from the thalamus to the cortex or the feedback from the cortex to the thalamus is delayed by a propagation time t_d. Here, ν_{ab} is the synaptic connection strength to population a from population b, and ϕ_n is the ascending input from brainstem, which can be white noise or any other arbitrary external signals, but here is set as constant for phase diagrams and bifurcation diagram. Figure 1(B) presents a schematic of these populations.

All populations except the excitatory population have very short axons, which lets us set $r_a \approx 0$ and $\gamma_a \approx \infty$ in (3), yielding $\phi_a = Q_a$ for $a = i, r, s$ [21]. Besides, intracortical connectivities are found to be proportional to the numbers of synapses involved [24], so one finds $V_e = V_i$ and $Q_e = Q_i$ [25], which allows us to concentrate on excitatory quantities, retaining inhibitory effects on the dynamics. Thus the model includes 16 parameters: $Q_{\max}$, θ', σ', α, β, γ_e, t_d, r_e, ν_{ee}, ν_{ei}, ν_{es}, ν_{se}, ν_{sr}, $\nu_{sn}\phi_n$, ν_{re}, ν_{rs}, which are enough to allow realistic representation of the most salient anatomy and physiology, but few enough to yield useful interpretations.

B. Spatially heterogeneous setting

Many previous studies of the corticothalamic system investigated its global (spatially uniform) dynamics; e.g., steady states, bifurcations from normal arousal states to epileptic seizures [21, 26, 27]. Specifically, bifurcations have been intensively investigated via changes of the parameter ν_{se}, which describes the excitatory influence of cortical pyramidal cells on the specific thalamic nuclei. It was chosen because of the prior implication of excitatory corticothalamic feedback in the pathophysiology of generalized absence and tonic-clonic seizures [8, 28–31]. Numerical investigation has demonstrated that this system provides a unified explanation for these two types of primary generalized seizures [21, 26]. Furthermore, recent analysis has established a bridge explicitly linking the tractable normal-form dynamical parameters with the underlying physiological parameters [27].

As for focal absence seizures in WAG/Rij rat model, the excitatory dendrites in focal region have larger total dendrite length, larger mean length of a dendritic segment and larger size of dendritic arbor, when data from within and outside epileptic area were compared [15, 16]. Additionally, in the focal cortical area, the excitatory-inhibitory ratio of neuron numbers is larger than that in other areas and the efficiency of GABA-ergic inhibition is reduced due to impairment [16]. What is more, lesion studies demonstrate that an excitable region is not sufficient for the occurrence of SWDs and indicate that some thalamic nuclei seem to be important for SWD occurrence [5]. So all the above suggest that we use the corticothalamic model with spatial heterogeneity on a 2D space (r_x, r_y), where the corticothalamic loops are distributed on each point $\boldsymbol{r}$, with periodic boundary conditions. This allows us to investigate the effect of local cortical connectivity and cortical propagation on the spatiotemporal dynamics, and to study how an initially focal seizure can be suppressed, localized, or propagate over the whole brain.

TABLE I. Nominal parameter values in spatially homogeneous model as studied in [26, 27].

Parameter	value	Unit	Parameter	value	Unit
$Q_{\max}$	250	s^{-1}	ν_{ee}	1.0	mV s
θ'	15	mV	$-\nu_{ei}$	1.8	mV s
σ	6	mV	ν_{es}	3.2	mV s
α	50	s^{-1}	$-\nu_{sr}$	0.8	mV s
β	200	s^{-1}	$\nu_{sn}\phi_n$	2.0	mV s
γ_e	100	s^{-1}	ν_{re}	1.6	mV s
t_d	40	ms	ν_{rs}	0.6	mV s

The above anatomical facts [15, 16] also validate that a higher value of ν_{se} in the focal area is suitable to describe the cortical seizure focus, with the parameter ν_{se} peaking at the center and smoothly decreasing to the edge, as shown in Fig. 2(A). For simplicity, its spatial profile is set as an isotropically symmetric Gaussian function

$$\nu_{se}(\boldsymbol{r}) = [\nu_{se}(0) - \nu_{se}(L/2)] \exp(|\boldsymbol{r}|^2/2\sigma^2) + \nu_{se}(L/2), \tag{9}$$

with σ characterizing the width and L being the system length. Figure 2(B) shows profiles along r_x at $r_y = 0$ with various σ. All other parameters are spatially invariant and given in Table I. The dynamics presented in results can be found over a wide range of parameters. This is one example.

Here, each spatial point represents a corticothalamic loop, and the corticothalamic system is set with a seizure focus surrounded by the normal region, characterized by two pathological parameters: σ and $\nu_{se}(0)$. The model provides a platform to study how the seizure focus can be suppressed, localized or propagate over the whole brain.

C. Simulation method

The model is simulated using the recently published NFTsim code written in C++ [32] to investigate the spatiotemporal dynamics [21, 26, 27]. It solves hyperbolic partial differential equations with delayed feedback such as the damped 2D wave equation in Eqs (3), (5)–(7). Numerical integration is performed using a fourth-order Runge-Kutta integrator. A cubic-spline interpolator is employed in order to estimate the time-delayed values of the midpoints required for the Runge-Kutta algorithm.

In the numerical simulation, the 2D space (r_x, r_y) is set as 120×120 grids with $L = 0.6$ m and $\delta r_x = \delta r_y = 0.5$ mm. Long (~ 1000 s) simulations are performed with a small time step ($\delta t = 0.1$ ms) to guarantee the system reaching its stationary state.

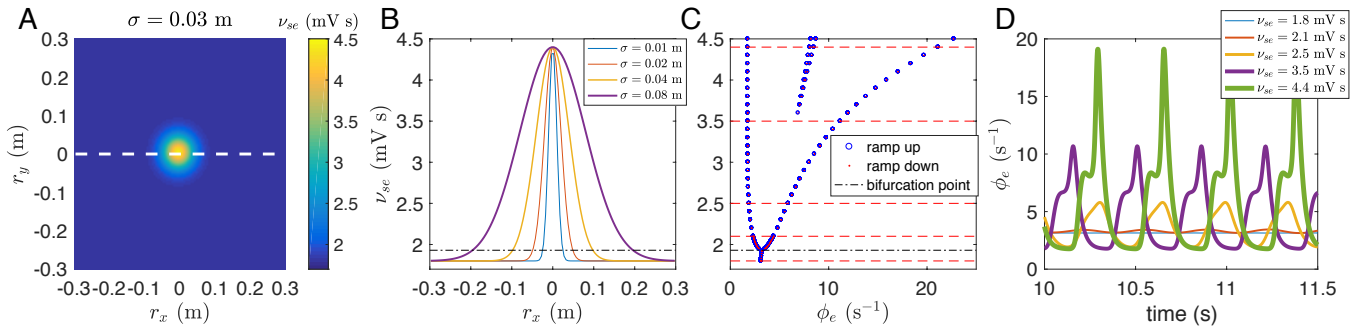

FIG. 2. (Color online) (A) Schematic of the 2D spatial model with periodic boundary conditions; The corticothalamic loop distributes at each position $\boldsymbol{r}$ with $\nu_{se}(\boldsymbol{r})$ determined by a spatially Gaussian profile given in Eq. (9) with a focal width σ, $\nu_{se}(L/2) = 1.8$ mV s and $\nu_{se}(0) = 4.4$ mV s. The white dashed line indicates the positions for spatiotemporal dynamics of ϕ_e shown in Fig. 4. (B) Spatially Gaussian profiles $\nu_{se}(\boldsymbol{r})$ along r_x at $r_y = 0$ with various σ. (C) Bifurcation diagram of ϕ_e when ν_{se} ramps up and down from $\nu_{se}(L/2)$ to $\nu_{se}(0)$ and *vice versa*. The black dashed line indicates the bifurcation point. (D) Time series of ϕ_e for various ν_{se} indicated by the red dashed lines in (C). Both (C) and (D) are the results for the spatially homogeneous case with all parameters spatially invariant.

Noise is ignored in the simulations for phase diagrams and bifurcation diagram, which simplifies our analysis, and focuses on the pattern formation and their underlying dynamical mechanisms. We have checked that a small noise has no significant effect on our findings here.

D. Steady states and linear stability analysis

To simplify the analysis, the system can be approximated to have a spatially radial symmetry, and then $\boldsymbol{r}$ can be replaced by $r = |\boldsymbol{r}|$. The system can be further rescaled to be dimensionless:

$$\hat{r} = r/r_e, \tag{10}$$

$$\hat{\sigma} = \sigma/r_e, \tag{11}$$

and then the spatial interaction in radial coordinates can be rewritten as the following normalized operator:

$$\text{Ł} = r_e^2\nabla^2 = \frac{\partial^2}{\partial\hat{r}^2} + \frac{1}{\hat{r}}\frac{\partial}{\partial\hat{r}}. \tag{12}$$

The stationary solutions converge to the solution at large r asymptotically, and the appropriate boundary condition at $\hat{r} = 0$ is

$$\partial\phi_a(0)/\partial\hat{r} = 0. \tag{13}$$

As proposed in Ref. [33], an instructive approach to obtain the steady states is to integrate Eqs (3), and (5)–(7) inward towards $\hat{r} = 0$, starting at a large $\hat{r}$, where the system can be linearized with $\hat{r}$ to be

$$\left[\text{Ł} - L_{CT}^{-1}(0,\hat{r})\right]\phi_e(\hat{r}) = 0, \tag{14}$$

with the function $L_{CT}^{-1}(\lambda,\hat{r})$ given in Appendix A, which describes the resonance [at $L_{CT}^{-1}(\lambda,\hat{r})$=0] of the corticothalamic loop for each spatial point $\hat{r}$ and each eigenmode with eigenvalue λ. One of its general solutions, decaying as $r \to L/2 \gg \sigma$, is

$$\phi_e(\hat{r}) = BK_0\left(\sqrt{L_{CT}^{-1}(0,\hat{r})}\hat{r}\right) + \phi_e(L/2), \tag{15}$$

where K_0 is a modified Bessel function of the second kind and B is an undetermined real constant. The choice of B uniquely parametrizes the stationary solution to the nonlinear equations (3), and (5)–(7). So our task is to search for the value of B for which the solution $\left[\phi_e^0(\hat{r}), V_e^0(\hat{r}), V_r^0(\hat{r}), V_s^0(\hat{r})\right]$ obeys the boundary condition (13) at $\hat{r} = 0$.

To analyze linear stability of the steady state, a small dimensionless perturbation can be introduced as follows:

$$\chi_a(\hat{r},t) = \left[\phi_a(\hat{r},t) - \phi_a^0(\hat{r})\right]/Q_{\max}, \tag{16}$$

$$v_a(\hat{r},t) = \left[V_a(\hat{r},t) - V_a^0(\hat{r})\right]\eta_a(\hat{r})/\sigma', \tag{17}$$

$$q_a(\hat{r},t) = \left[Q_a(\hat{r},t) - Q_a^0(\hat{r})\right]/Q_{\max}, \tag{18}$$

with $\sigma' = \sigma\sqrt{3}/\pi$, $\eta_a(\hat{r}) = q_a^0(\hat{r})\left[1 - q_a^0(\hat{r})\right]$, and $q_a^0(\hat{r}) = Q_a^0(\hat{r})/Q_{\max}$ for $a = e, r, s$. The perturbations can be expanded in sums of eigenmodes as follows:

$$\chi_e(\hat{r},t) = \sum_i C_i \exp(\lambda_i t)\hat{\chi}_e(\lambda_i,\hat{r}), \tag{19}$$

$$q_a(\hat{r},t) = \sum_i C_i \exp(\lambda_i t)\hat{q}_a(\lambda_i,\hat{r}), \tag{20}$$

each of which obeys

$$\left[\text{Ł} - L_{CT}^{-1}(\lambda_i,\hat{r})\right]\hat{\chi}_e(\lambda_i,\hat{r}) = 0, \tag{21}$$

one of whose general solutions for $\hat{r} \to \infty$ is

$$\hat{\chi}_e(\lambda_i,\hat{r}) = K_0\left(\sqrt{L_{CT}^{-1}(\lambda_i,\hat{r})}\hat{r}\right). \tag{22}$$

Note that there is no constant B as in the steady state equation (15), because B can be included in C_i. So now

our task is to search for the eigenvalue λ_i as well as the corresponding perturbation eigenmode. The largest real part value of all λ_i determines linear stability of the steady state.

III. RESULTS

The corticothalamic system with an initial seizure focus is investigated by numerical simulations to study how the cortical propagation can suppress, localize, or generalize the seizure focus in Sec. III A and III B, exploring the phase diagram of spatiotemporal dynamics. In Sec. III C, traveling waves that emerge from the focus in various phases are investigated, yielding predictions to be further tested experimentally. Then the underlying dynamical mechanisms for various phases are uncovered in Sec. III D using eigenvalue spectra and corresponding eigenmodes at critical points. Finally, Sec. III E shows robustness of the dynamical mechanism for the emergence of seizure localization.

A. From seizure suppression to seizure generalization

In the homogeneous case, the system has a spatially uniform activity and the corticothalamic loop experiences a supercritical Hopf bifurcation from normal states to absence seizures, then a period-doubling, in the selected range of ν_{se} from $\nu_{se}(L/2)$ to $\nu_{se}(0)$, as shown in the bifurcation diagram of Fig. 2(C). In Fig. 2(D), various dynamical states of the corticothalamic loop are shown by time series of ϕ_e at various ν_{se}, whose values are correspondingly indicated by the red dashed line in Fig. 2(C). Specifically, one can find the oscillating dynamics with ~ 3 Hz rhythm and the stereotyped SWDs. This result has been compared with clinical data in details and thus was employed to explain the pathological transition from normal arousal state to the generalized absence seizure [21, 26].

To study the effect of the spatial extension of an initial seizure focus on the oscillating rhythms, we investigate the focal width σ relative to the intrinsic axon spatial range r_e of the system. Actually, σ can be rescaled by r_e as in Eq. (11), but both of them are constrained by the system size L, which imposes edge effects on the spatiotemporal dynamics. Thus, in the following, various spatiotemporal dynamics induced by the seizure focus are investigated in r_e–σ parameter space.

The phase diagram in Fig. 3 shows various spatiotemporal dynamical phases. Firstly, large r_e, as in the case of healthy adults [34], facilitates the normal region to suppress the seizure focus with small size σ, referred as Phase I: seizure suppression. With the seizure focus suppressed, the activity profile stabilizes with a little higher activity in the center, as shown in Fig. 4(A). Secondly, if the seizure focus has an enough large size σ to resist

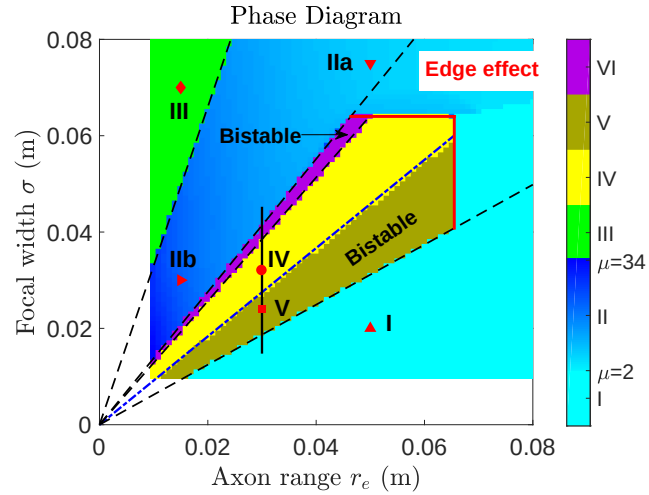

FIG. 3. (Color online) Phase diagram of spatiotemporal dynamics in r_e–σ parameter space with six phases: I, seizure suppression; II, attenuated theta wave; III, inward theta wave; IV, modulated alpha wave; V, bistable phase with seizure suppression and regular alpha wave; VI, bistable phase with modulated alpha wave and attenuated theta wave; Six examples are indicated by various shaped red points, with the corresponding spatiotemporal dynamics of ϕ_e shown in Fig. 4. They are successively separated by the black dashed or the blue dash-dotted lines, the latter of which indicates the instability line for ~ 10 Hz oscillation, as well predicted by linear stability analysis. The attenuation factor μ in unit of m^{-1} for Phase II is also indicated in the colorbar. Note that edge effects stop further extension of Phase IV, V, and VI, which can be relaxed in the system with larger size; e.g., $L = 1$ m (not shown here). The black vertical line indicates the parameter range for further investigation in Fig. 5. Numerical simulation in the left and bottom white band would require much longer simulation time.

the suppression, and can even propagate over the whole system, then the absence seizure generalizes, as in the common case of primary generalized absence seizure as studied in [21, 26], referred here as Phase II: seizure generalization. In this case, seizure activity originates from a temporally oscillating center and propagates rapidly outward to the whole system, but with the wave amplitude attenuated along r, as shown in Fig. 4(B) and (C). It can be characterized by the attenuation factor $\mu = \partial \log \phi_e(r)/\partial r$ with unit of m^{-1}, whose values are also indicated in Fig. 3. One can find it largely depends on r_e, with larger attenuation at smaller r_e. Here the system transits continuously from seizure suppression to seizure generalization via a supercritical Hopf bifurcation with the oscillating amplitude increasing from 0 gradually. Such transition is indicated in upper right corner of Fig. 3, where the system size constrain leads to edge effects. Furthermore, small r_e reverses the direction of propagating waves from outward in Phase II to inward as in Phase III, whose wave dynamics is presented in Fig. 4(D). The reversion from outward to inward can be understood by the analysis of front wave instability [35],

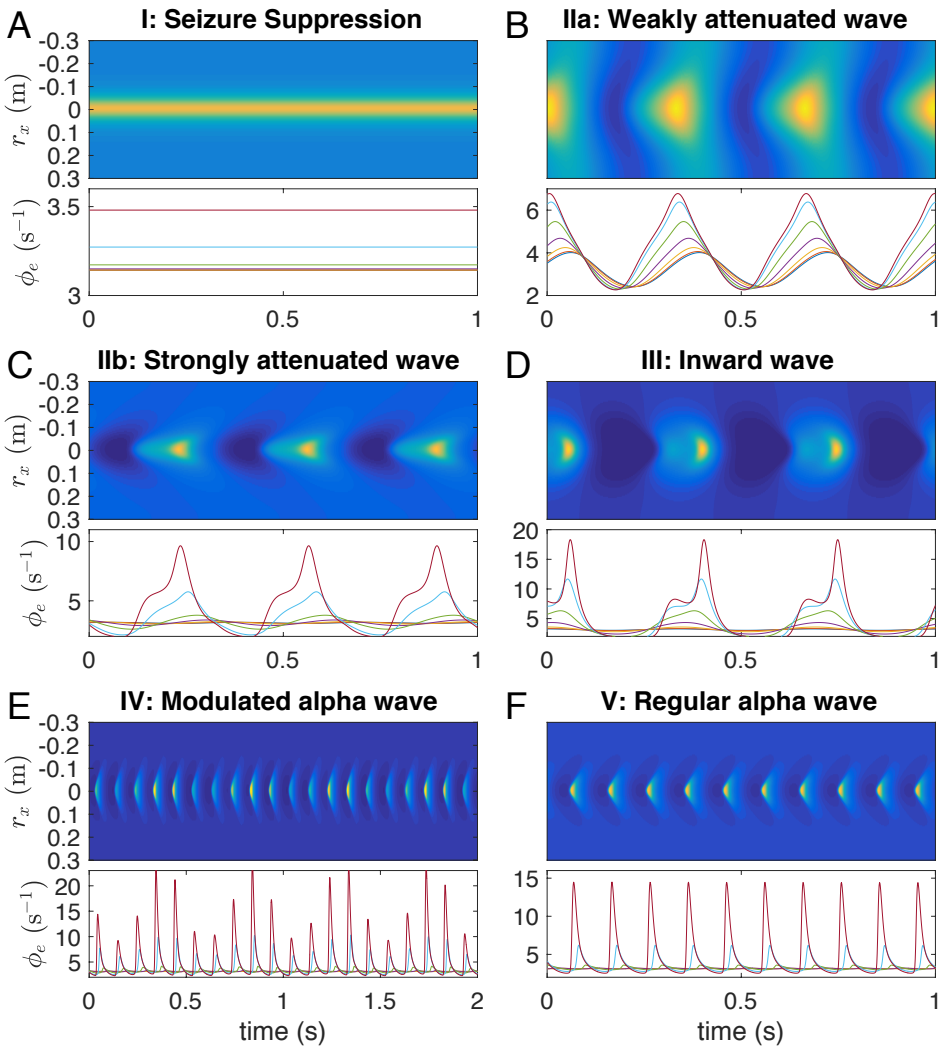

FIG. 4. (Color online) Examples of various waves with parameter values of (r_e, σ) indicated by the corresponding shaped red points in Fig. 3. all waves are radially symmetrical, and therefore only 1D wave dynamics is presented. The upper panel presents the 1D wave dynamics of points at $r_y = 0$, also indicated as the white dashed line in Fig. 2(A), while the lower panel shows the corresponding time series at equispaced points from center to edge with decreasing base level of ϕ_e (for I) or its amplitude (for II–V). (A) Phase I, seizure suppression. (B) Phase IIa, the wave weakly attenuated along $\boldsymbol{r}$. (C) Phase IIb, the wave strongly attenuated along $\boldsymbol{r}$. (D) Phase III, the wave propagating inward from edge to the center, in contrast with that in Phase II, where waves are propagating outward from center to edge. (E) Phase IV, the spatially localized alpha wave modulated by ~ 2 Hz slow wave. (F) One state in Phase V: the spatially localized regular alpha wave, which coexists with seizure suppression.

which is beyond our focus here.

B. Emergence of seizure localization

Interestingly, the initial seizure focus can induce an alpha wave with ~ 10 Hz rhythm, referred as Phase IV. Such high amplitude alpha wave was used to explain the generalized tonic-clonic seizure [26], but here emerges due to an initial absence seizure focus. As shown in the upper panel of Fig. 4(E), the alpha wave is spatially localized with no oscillating activity in the normal region, in contrast with the traveling wave over the whole system in seizure generalization (see the upper panel of Fig. 4(B)–(D)). Figure 4(E) also shows that it is temporally modulated by a ~ 2 Hz slow wave. Such temporal modulation is reminiscent of complex-partial seizures with consciousness impaired [36, 37], which have significantly increased delta-range 1–2 Hz slow wave activity in the bilateral frontal and parietal neocortex compared with simple-partial seizures, where consciousness is not impaired. Thus such temporally modulated and spatially localized alpha wave may serve as an underlying mechanism for complex-partial seizure generation. So it is worth further investigating the underlying biophysical mechanism for such a robust ~ 2 Hz modulation in

future, which is beyond our focus of this work.

The modulation here is due to the nonlinear effect after its emergence, as indicated in Fig. 5 of the bifurcation diagram, which shows that the dynamical trajectory of each spatial point experiences a quasiperiodic cycle. With increasing σ, the oscillating waveform becomes increasingly complex and destabilized via a second Hopf bifurcation to more complex dynamics on a 2-torus, 3-torus, then to higher dimensional dynamics, to a chaotic attractor, as indicated by a window for period 3 in the bifurcation diagram. Such route to a chaotic attractor has also been observed in the homogeneous corticothalamic system [27]. The bifurcation diagram in Fig. 5 also shows a sudden transition from seizure suppression to seizure localization via a subcritical Hopf bifurcation with hysteresis. After the transition, the system reaches a large amplitude localized alpha wave, as shown in Fig. 4(E). The hysteresis accompanies the bistable region referred to as Phase V, where seizure suppression coexists with seizure localization, which has a localized regular alpha wave as shown in Fig. 4(F). Such emerged bistability originates from pathological pattern formation, which provides a new route for the transition from normal states to epileptic activity [4, 38]. What is more, the bifurcation diagram shows another bistable region referred as Phase VI: coexistence of seizure localization with seizure generalization. This predicts that the spatially localized chaotic dynamics can coexist with the spatially generalized but regular traveling wave, although it happens in a narrow parameter region and may be hard to detect in experiments. Nonetheless, the spatially localized waves in Phase IV, V, and VI terminate at large σ and r_e due to edge effects, but can otherwise extend further in a system with larger size.

Localized waves in Phases IV, V, and VI can be described as breathers. It emerges after the seizure suppression in Phase I becomes unstable and the instability boundary can be well predicted by linear stability analysis, as indicated by the blue dash-dotted line in Fig. 3. All other boundaries of phases beyond edge effect are also fully determined by the normalized focal width $\hat{\sigma} = \sigma/r_e$ (the dashed lines in Fig. 3). Thus, our results hold for general scenarios with various spatial scales; e.g., various axon range r_e, whenever there is no edge effect, and can be specially applied in the scenario with multiple seizure focuses, which spread widely but do not interact.

C. Travelling wave properties

Propagating waves of electrical activity have been observed in numerous mammalian systems and during seizures in rats and in cats [39]. Various wave velocities were estimated ranging from 0.01 to 10 m s^{-1}, dependent on the cortical states and methods of data analysis [20, 39].

Here, we characterize the wave propagation by phase velocity v_p, which can be calculated by differentiating the

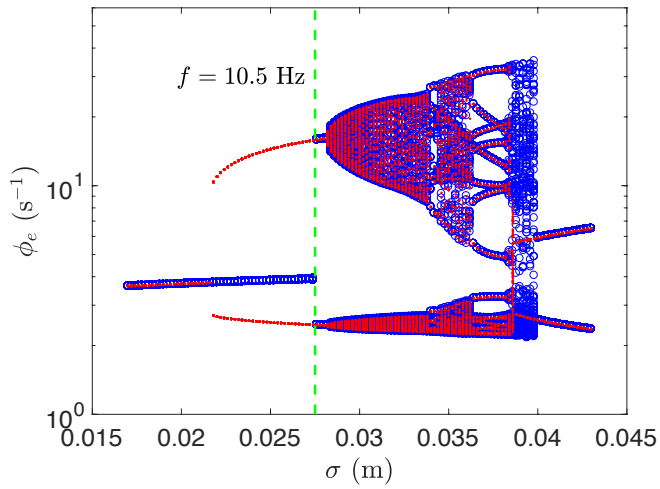

FIG. 5. (Color online) Bifurcation diagram of ϕ_e at ($r_x = 0, r_y = 0$) against σ, with two bistable regions, corresponding to Phase V&VI, respectively. The critical point for bifurcation from seizure suppression to the localized alpha wave with rhythm $f = 10.5$ Hz is consistent with linear stability analysis, as indicated by the green dashed line. Blue circle, ramp up; red dot, ramp down; $r_e = 0.03$ m.

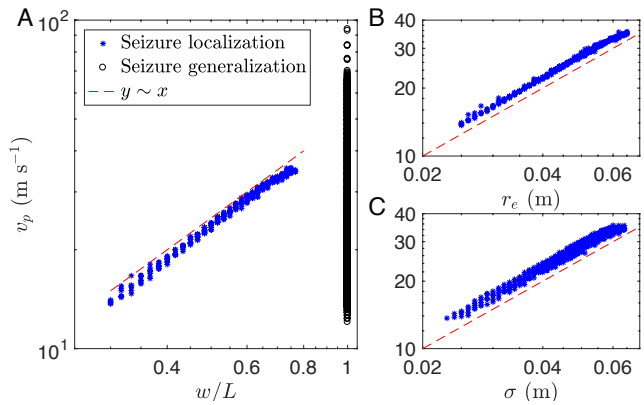

FIG. 6. (Color online) Wave velocity v_p. (A) v_p *vs.* w/L in both seizure generalization and seizure localization; (B) v_p *vs.* r_e; (C) v_p *vs.* σ; The linear behavior for seizure localization is a prediction for further experimental test.

dynamical phase with the space, over the whole system for seizure generalization, but limited in the seizure region for seizure localization. The seizure region is defined with its oscillating amplitude at any spatial point not less than 0.03 times of the maximal amplitude in the seizure focus. From Fig. 6, the seizure focus with ~ 3 Hz rhythm in seizure generalization propagates over the whole system at the velocity ranging from 10 to 100 m s^{-1}, while the seizure focus with ~ 10 Hz rhythm in seizure localization spreads within the seizure region at the velocity ranging from 13 to 33 m s^{-1}. What is more, the latter phase velocity v_p linearly depends on the width w of the defined seizure region, when the seizure width w with re-

spect to the system width L ranges from 0.3 to 0.8, as shown in Fig. 6 (A). Such linear dependence is consistent with the robust rhythm of the localized wave, which is irrespective to the parameters: r_e and σ. Because there is only one stripe at any instant, that is the wave has only one peak along the radius r, as demonstrated in the upper panel of Fig. 4(E) and (F) as well as in their eigenmodes in Sec. III D. Actually, the wave velocity also linearly depends on both σ and r_e, as shown in Fig. 6(B) and (C). So both σ are r_e are combined to determine the linear behavior in seizure localization. These findings provide a theoretical prediction for further experimental tests.

Therefore, our model here provides a theoretical framework to generate seizure acitivities with spatiotemporal dynamical features matching well with experimental wave rhythms and spatial extensions for global and focal absence epilepsy, respectively.

D. Dynamical mechanism underlying emergence

In our previous work, ~ 3 Hz theta waves and ~ 10 Hz alpha waves were generated due to the resonance of two different delayed feedback loops: $e \to r \to s \to e$ or $e \to s \to e$, respectively, in the homogeneous corticothalamic system [21, 26, 27]. So, it is not clear whether the localized alpha wave originates from the resonance of the same underlying corticothalamic loop, as in the homogeneous system, or is induced by the seizure focus responsible for the ~ 3 Hz rhythm.

To clarify the underlying dynamical mechanism for the emergence of such localized alpha waves, we now investigate steady states and their corresponding eigenvalue spectra, summarized in Fig. 7. Figure 7(A) and (B) show the three eigenvalues with largest real part, varying with the focal width σ. The linear stability is determined by the eigenvalue with largest real part. In Figs. 7(A) and (B), the blue one corresponds to the localized alpha wave with frequency $f = 10.5$ Hz and the green ones for the generalized theta wave with frequency $f = 3.1$ Hz, respectively.

We focus on the following three typical scenarios: (i) Seizure suppression ($\sigma = 0.024$ m); (ii) Seizure localization ($\sigma = 0.032$ m); (iii) Seizure generalization ($\sigma = 0.040$ m), with their corresponding steady states and eigenvalue spectra shown in Figs. 7(C)–(H). Firstly, Fig. 7(C) and (D) show that the analytical solution of the stable steady state is consistent with numerical simulations for seizure suppression. Their excellent match verifies the assumption of radial symmetry and infinite system size, and lends confidence for our further analysis. Secondly, in Fig. 7(E), the steady state with larger σ becomes unstable in seizure localization, as indicated by one eigenvalue with a positive real part (the rightmost blue star in Fig. 7(F)). Here, seizure focus is localized because σ is not large enough to spread the wave over the whole system, but is large enough to free the seizure focus from being suppressed by the surrounding normal region. As a result, a breather emerges, with its steady state still stable at the tail, but unstable at the focal region. Finally, with σ further increased, the steady state at the tail becomes unstable with one eigenvalue along with the bottom branch crossing the imaginary axis in Fig. 7(H), and the theta wave originating from the focal region propagates over the whole system. Nonetheless, Fig. 7(G) shows the time-averaged activity is consistent with the steady state, indicating that the spatiotemporal activity oscillates around the steady state via a supercritical Hopf bifurcation.

The dynamical picture is consistent with that indicated in eigenvalue spectra. In Fig. 7(D),(F) and (H), it shows that most eigenvalues (green stars) align with two branches, where $L_{CT}^{-1}(\lambda, \infty)$ is real negative ($L_{CT}^{-1}(\lambda, \infty) = 0$ at the branch end). These two eigenvalue branches correspond to the resonance of two delayed feedback loops, respectively, as in the spatially homogeneous corticothalamic system [21, 27]. It is a general property in the delayed system that an infinite number of eigenvalues will align with such branches. Generally, the delay leads the spectrum of the system to be determined by a Lambert function [40]:

$$W(\lambda) \exp[W(\lambda)] = \lambda, \tag{23}$$

where $W(\lambda)$ is a complex function with an infinite number of solutions. So here most dynamical eigenmodes correspond to the potential resonance of the underlying corticothalamic loops as that in the spatially homogeneous corticothalamic system.

However, it is appealing that some eigenvalues indicated as blue stars in Figs. 7(D),(F) and (H) emerge beyond the last two branches, implying that their eigenmodes are not purely induced by the resonance of the underlying corticothalamic loops. For these eigenmodes, $L_{CT}^{-1}(\lambda, \infty)$ has a much larger value than that for eigenvalues (green stars) close to the two branches. That means the steady state at the tail will stay stable, and is not easy to be driven to have a corticothalamic loop resonance. But the system's steady state becomes unstable as indicated in Fig. 7(F) with a positive real part of the eigenvalue. Thus, such eigenmode is confined in some focal region, as confirmed in Figs. 8(A) and (B). As a result, it emerges another wave with its frequency and waveform different from the original theta wave in seizure generalization. What is more, this eigenmode is also spatially confined by its steady state, as shown in Figs. 8(A) and (B). This is in contrast with the eigenmode in seizure generalization, as shown in Fig. 8(C) and (D), where the wave propagates outwards from the focal area, but the activity at each spatial point still surrounds its steady state.

Thus the emergence of the localized alpha wave is due to spatial confinement and the resulted spatial dispersive resonance, different from the corticothalamic loop resonance in the spatially homogeneous system [21, 26, 27]. Such underlying dynamical mechanism also explains why edge effects can terminate the emergence of seizure lo-

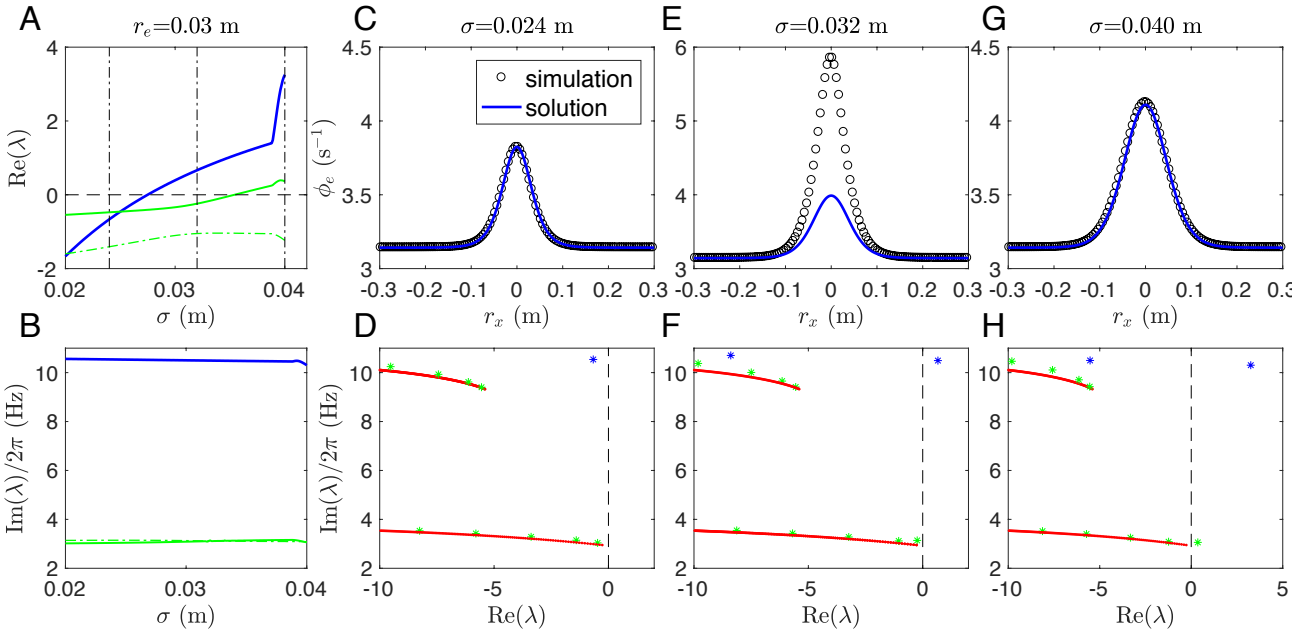

FIG. 7. (Color online) Steady states and their eigenvalue spectra. (A) Re(λ) *vs.* σ at $r_e = 0.03$ m for 3 eigenvalues with largest real part. Three vertical dash-dotted black lines indicate the values of σ for further analysis in (C)–(F). (B) Corresponding Im(λ) *vs.* σ as in (A). (C) Stable steady state at $\sigma = 0.024$ m; (D) Corresponding rightmost eigenvalues at $\sigma = 0.032$ m. (E) Unstable steady state evolves to localized alpha wave at $\sigma = 0.032$ m; (F) Corresponding rightmost eigenvalues at $\sigma = 0.032$ m. (G) Unstable steady state evolves to theta wave at $\sigma = 0.040$ m; (H) Corresponding rightmost eigenvalues at $\sigma = 0.040$ m. Steady states are compared between the time averaged 1D spatial profile from simulations and the numerical solutions obtained from integration of Eq. (14) in (C), (E), and (G); Note that many eigenvalues (green stars) except few ones (blue stars) align with two branch cuts (red lines, where $L_{CT}^{-1}(\lambda, \infty)$ is real negative), indicating that most dynamical eigenmodes tend to generalize the focal seizure, but there are also some new emerging eigenmodes (blue stars) to localize the seizure focus and the localized oscillation is due to the resulted spatial dispersive resonance.

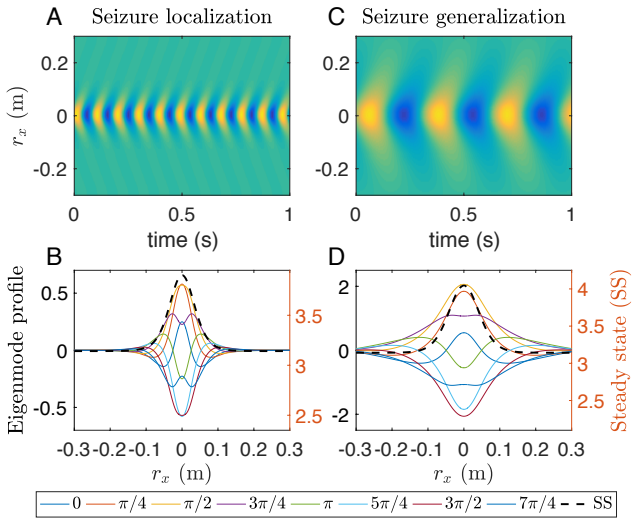

FIG. 8. (Color online) Spatiotemporal eigenmodes of alpha wave and theta wave at the respective critical point for $r_e = 0.03$ m: (A, B) $\sigma = 0.0275$ m; (C, D) $\sigma = 0.0354$ m. (A, C) 1D wave dynamics of ϕ_e for points at $r_y = 0$; (B, D) 1D spatial profile of ϕ_e for both eigenmodes and the corresponding steady states at $r_y = 0$ and various instantaneous phases φ_0, as indicated in the bottom legend.

calization, because there is no enough space to confine it with a firm boundary. Furthermore, such spatially confined eigenmode in Figs. 8(A) and (B) is also unstable and then evolve to another localized alpha wave with a much higher amplitude, which is beyond the steady state in phase space, as shown in Fig. 7(E). So seizure localization emerges via a subcritical Hopf bifurcation, jumping from seizure suppression.

E. Robustness of dynamical mechanism

The above dynamical mechanism for the emergence of seizure localization is robust without requirement of parameter fine-tuning. A large parameter region is found in Fig. 9(A) and (B) for seizure localization, which occurs as long as the focal seizure activity is too unstable to be suppressed by normal region with the parameter $\nu_{se}(0)$ large enough to be far away from the linear stability boundary of the corticothalamic loops (the critical value $\nu_{se}^c \approx 1.98$ mV s, also indicated in Fig. 2(C)). In Fig. 9(A), it also shows that seizure suppression can transit to seizure generalization, when $\nu_{se}(0)$ is not large enough. This is the weak nonlinear case explored in [41], where the effect of system size is ignored. So the emer-

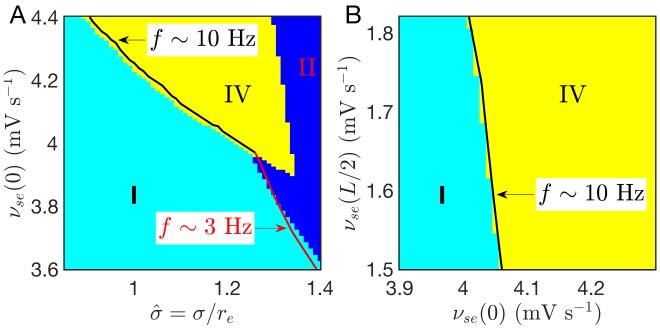

FIG. 9. (Color online) Emergence of seizure localization due to highly nonlinear effect of focal seizure activity. (A) Phase diagram on [$\hat{\sigma}$, $\nu_{se}(0)$]; (B) Phase diagram on [$\nu_{se}(0)$, $\nu_{se}(L/2)$] with $\hat{\sigma} = 1.2$. $\nu_{se}(L/2)$ has a much weaker effect on the emergence, in consistent with its underlying dynamical mechanism in Sec. III D. The linear instability boundaries are well predicted by linear stability analysis.

gence is due to nonlinear effect as well as the spatially dispersive resonance.

The emergence also requires the normal region to be stable enough to be evoked by the seizure focus. However, Fig. 9(B) shows that $\nu_{se}(L/2)$ has a much weaker effect for the emergence. This is consistent with its underlying dynamical mechanism as explained in Sec. III D, since, the normal region in seizure localization is already stable and has established a firm boundary, further lowering $\nu_{se}(L/2)$ to make the normal region more stable will make little contribution. This finding can also be tested in experiments.

The simulation results are also confirmed by linear stability analysis, as shown in Fig. 9, indicating that the parameter selection for the dynamical mechanism in pathological pattern formation is not unique, but general, whenever the system has strong nonlinear activity in the focal area and the conditions for spatially dispersive resonance are satisfied.

IV. SUMMARY AND DISCUSSION

To summarize, we propose here the pathological pattern formation to unify global and focal absence seizures, using a physiology-based corticothalamic model with an initial seizure focus. We found that the interlay between cortical propagation and the underlying corticothalamic circuit can generate various spatiotemporal dynamics: seizure suppression, seizure generalization and seizure localization, mainly dependent on the relative size of focal width σ with respect to both the axon spatial extension r_e and the system size L. In seizure generalization, the focal seizure propagates fast outward over the whole system with ~ 3 Hz rhythm, while in seizure localization, a spatially localized alpha wave with ~ 10 Hz rhythm emerges with a higher amplitude. These self-organized waves are robust and agree well with experimental wave rhythms and spatial extensions during seizures for both global and focal aspects. Their underlying dynamical mechanisms are as well explained in details through eigenvalue spectra and corresponding eigenmodes at critical states. Therefore, our results here provide a biophysical and mechanistic explanation of higher frequency and amplitude of the waves observed in genetic rat models with absence epilepsy, and imply that global and focal absence epilepsy could be unified in the theoretical framework of pathological pattern formation.

Our results also present several predictions for further experimental tests:

(i) The 7–11 Hz wave in WAG/Rij model may be explained by an effective short axon length r_e on cortex (spatially effective propagation length), which should be further tested in experiments. In humans, r_e may be large enough to make the system act in the region with edge effect, and therefore induce seizure generalization with seizure focal activity spreading over the whole system.

(ii) The alpha wave in seizure localization can be modulated by a ~ 2 Hz slow wave and its phase propagation velocity linearly depends on the focal seizure size.

(iii) Seizure localization can coexist with seizure generalization.

(iv) The state in normal region has a weak effect on suppressing the focal seizure.

Here, we focus on the interplay of the cortical propagation and the underlying corticothalamic loop, which is beyond most previous work about spatially extended heterogeneous cortical model, employed to investigate the effect of cortical diffusion on the seizure activity and their transitions as well as transient dynamics [42–45]. The emergence of breathers in seizure localization has also been explored in previous work, which was discussed in an abstract neural field model with Maxico hat connection profile and also some adaptive feedback, such as spike-frequency adaptation and so on [46–48]. Theoretically, the sigmoid function is simplified to a step function, easing linear stability analysis and feasibly employing the Evans function [35, 49]. Here, we keep the sigmoid function, excluding the possibility to use the Evans function for eigenvalue spectra. But, our corticothalamic model here is tractable especially via a formulation in terms of differential equations, physiologically justifiable, and relies on parameters that are experimentally measurable. So our results here can be related back to the physiological effects.

It has also been widely explored that how the SWDs in absence seizures can be more robustly produced by involving a second slow inhibitory population or inhibitory variable with a slower time scale, such as GABA$_B$ [50]. The relative contribution of both fast GABA$_A$ and slow GABA$_B$ receptor-mediated inhibitions has been discussed a bit for controlling absence seizures [51]. A reduction of the contribution of GABA$_A$ and an increase of that of GABA$_B$ can slow down the paroxysmal oscillations and increase their amplitudes. On the other hand,

the effect of basal ganglia (BG) is proposed to be important for maintaining absence seizures over several tens of seconds by the dynamical loop of the BG-thalamocortical network [52], which also provides a modulation site and a pathway to prevent absence seizures [53, 54]. But, up to now, less is know about the effect of the cortical spatial extension and the cortical local connectivities. Thus, our work here provide a new route for absence seizure controlment in future.

Our work here just considers the short-range intracortical connections. Recently, the combination of short-range and long-range spatial connectivity kernels is proposed to be critical for synchronous seizure termination, which is a commonly observed phenomenon during seizures [55]. Therefore, our corticothalamic model can be further extended with heterogeneous long-range spatial connectivity to study seizure onset, propagation as well as termination.

As to the underlying dynamical mechanisms, the type of Hopf bifurcation for the transition from seizure suppression to seizure localization or seizure generalization can be more systematically studied by employing the normal form theory [27]. The canonical nature in the sense of normal form theory is not rigorously justified for the spatiotemporal evolution equations, which is mathematically significantly less developed. But with some special perturbation mode, it can still be used to understand the effects of other biophysical properties on the bifurcation type, such as the bursting activities in thalamic populations, the slow dynamics of extracellular $[\mathrm{K}+]_0$ concentration, as well as the spike frequency adaptation.

ACKNOWLEDGMENTS

This work was supported by the Australian Research Council Center for Integrative Brain Function (Grant CE140100007) and by Australian Research Council Laureate Fellowship Grant FL140100025.

Appendix A: Derivation of $L_{CT}(\lambda, \hat{r})$

Here we present the derivation of the radially symmetric linear operator $L_{CT}(\lambda, \hat{r})$ for each spatial point of the corticothalamic system and each eigenmode corresponding to eigenvalue λ. $\lambda = 0$ is for the stationary solution in Eqs (14) and (15) and others for general eigenmodes in Eqs (21) and (22). $L_{CT}(\lambda, \hat{r})$ for both cases are derived when a small perturbation is imposed on a given steady state, either $[\phi_e^0(\infty), V_e^0(\infty), V_r^0(\infty), V_s^0(\infty)]$ or $[\phi_e^0(\hat{r}), V_e^0(\hat{r}), V_r^0(\hat{r}), V_s^0(\hat{r})]$. Here the general perturbation with eigenvalue λ at position $\hat{r}$ is denoted as $[\hat{\phi}_e, \hat{V}_e, \hat{V}_r, \hat{V}_s]$, where $(\lambda, \hat{r})$ is ignored for simplicity, which yields

$$[D(\lambda) - \mathbf{Ł}]\,\hat{\phi}_e = \hat{Q}_e, \tag{A1}$$

$$\hat{V}_e = L(\lambda)\left[\nu_{ee}\hat{\phi}_e + \nu_{ei}\hat{Q}_e + \nu_{es}\hat{Q}_s E(\lambda)\right], \tag{A2}$$

$$\hat{V}_r = L(\lambda)\left[\nu_{re}\hat{\phi}_e E(\lambda) + \nu_{rs}\hat{Q}_s\right], \tag{A3}$$

$$\hat{V}_s = L(\lambda)\left[\nu_{se}(\hat{r})\hat{\phi}_e E(\lambda) + \nu_{sr}\hat{Q}_r\right], \tag{A4}$$

with

$$E(\lambda) = \exp(-\lambda t_d), \tag{A5}$$

$$D(\lambda) = (1 + \lambda/\gamma_e)^2, \tag{A6}$$

$$L(\lambda) = (1 + \lambda/\alpha)^{-1}(1 + \lambda/\beta)^{-1}. \tag{A7}$$

By linearizing the sigmoid function near the steady state, Eqs (A2)–(A4) can give us the following relationship between $\hat{Q}_e$ and $\hat{\phi}_e$:

$$\hat{Q}_e = [x + y_s z_s]\,\hat{\phi}_e, \tag{A8}$$

with

$$x = \frac{J_{ee}}{1 - J_{ei}}, \tag{A9}$$

$$y_s = \frac{J_{es}}{1 - J_{ei}}, \tag{A10}$$

$$z_s = \frac{J_{se} + J_{sre}}{1 - J_{srs}}, \tag{A11}$$

where $J_{abc} = J_{ab}J_{bc}$, $J_{ab}(\lambda, \hat{r}) = G_{ab}(\hat{r})L(\lambda)$ for connections within cortex or thalamus, $J_{ab}(\lambda, \hat{r}) = G_{ab}(\hat{r})L(\lambda)E(\lambda)$ for connections between cortex and thalamus with time delay t_d. Here x, y_s, and z_s are the signal transductions along axons from cortical field to cortex, from thalamic relay nucleus to cortex, and from cortical field to thalamic relay nucleus, respectively, as shown in Fig. (2) of reference [27]. The gain $G_{ab}(\hat{r}) = \nu_{ab}\eta_a(\hat{r})Q_{\max}/\sigma'$ is the additional output produced by neurons a per unit additional input from neurons b. ν_{ab}, G_{ab} and J_{ab} are indicated in Fig. 1(B). Thus $L_{CT}(\lambda, \hat{r})$ can be expressed as

$$L_{CT}^{-1}(\lambda, \hat{r}) = D(\lambda) - x(\lambda, \hat{r}) - y_s(\lambda, \hat{r})z_s(\lambda, \hat{r}), \tag{A12}$$

which at $L_{CT}^{-1}(\lambda, \hat{r})$=0 yields the resonance of the corticothalamic loop for each radial distance $\hat{r}$ and each eigenmode with eigenvalue λ.

[1] V. Crunelli and N. Leresche, Nat. Rev. Neurosci. **3**, 371 (2002).

[2] R. S. Fisher and D. A. Prince, *Electroencephalography and Clinical Neurophysiology*, Clin. Neurophysiol. **42**,

608 (1977).
[3] A. Destexhe, J. Neurosci. **18**, 9099 (1998).
[4] F. L. D. Silva, W. Blanes, S. N. Kalitzin, J. Parra, P. Suffczynski, and D. N. Velis, Epilepsia **44**, 72 (2003).
[5] H. K. Meeren, J. G. Veening, T. A. Möderscheim, A. M. Coenen, and G. van Luijtelaar, Exp. Neurol. **217**, 25 (2009).
[6] M. Avoli, Epilepsia **53**, 779 (2012).
[7] A. Depaulis and S. Charpier, Neurosci. Lett. **667**, 53 (2018).
[8] H. K. M. Meeren, J. P. M. Pijn, E. L. J. M. van Luijtelaar, A. M. L. Coenen, and F. H. Lopes da Silva, J. Neurosci. **22**, 1480 (2002).
[9] E. Sitnikova and G. van Luijtelaar, Brain Research **1012**, 127 (2004).
[10] P.-O. Polack, I. Guillemain, E. Hu, C. Deransart, A. Depaulis, and S. Charpier, J. Neurosci. **27**, 6590 (2007).
[11] P.-O. Polack, S. Mahon, M. Chavez, and S. Charpier, Cereb. Cortex **19**, 2078 (2009).
[12] H. K. M. Meeren, G. van Luijtelaar, F. H. Lopes da Silva, and A. M. L. Coenen, JAMA Neurol. **62**, 371 (2005).
[13] M. D. Holmes, M. Brown, and D. M. Tucker, Epilepsia **45**, 1568 (2004).
[14] H. Blumenfeld, Epilepsia **46**, 21 (2005).
[15] G. van Luijtelaar and E. Sitnikova, Neurosci. Biobehav. Rev. **30**, 983 (2006).
[16] A. M. L. Coenen and E. L. J. M. van Luijtelaar, Behav. Genet. **33**, 635 (2003).
[17] F. L. da Silva, A. van Rotterdam, W. S. van Leeuwen, and A. Tielen, Electroencephalogr. Clin. Neurophysiol. **29**, 260 (1970).
[18] P. Robinson, J. Theor. Biol. **222**, 163 (2003).
[19] M. C. Cross and P. C. Hohenberg, Rev. Mod. Phys. **65**, 851 (1993).
[20] M. A. Kramer, H. E. Kirsch, and A. J. Szeri, J. Royal Soc. Interface **2**, 113 (2005).
[21] P. A. Robinson, C. J. Rennie, and D. L. Rowe, Phys. Rev. E **65**, 041924 (2002).
[22] V. K. Jirsa and H. Haken, Phys. Rev. Lett. **77**, 960 (1996).
[23] P. A. Robinson, C. J. Rennie, and J. J. Wright, Phys. Rev. E **56**, 826 (1997).
[24] V. Braitenberg and A. Schüz, *Cortex: statistics and geometry of neuronal connectivity* (Springer Science & Business Media, 2013).
[25] J. J. Wright and D. T. J. Liley, Behav. Brain Sci. **19**, 285 (1996).
[26] M. Breakspear, J. A. Roberts, J. R. Terry, S. Rodrigues, N. Mahant, and P. A. Robinson, Cereb. Cortex **16**, 1296 (2006).
[27] D.-P. Yang and P. A. Robinson, Phys. Rev. E **95**, 042410 (2017).
[28] A. Destexhe and T. J. Sejnowski, *Thalamocortical assemblies* (Oxford: Oxford University Press, 2001).
[29] D. A. McCormick and D. Contreras, Annu. Rev. Physiol. **63**, 815 (2001).
[30] H. Nersesyan, F. Hyder, D. L. Rothman, and H. Blumenfeld, J. Cereb. Blood Flow Metab. **24**, 589 (2004), pMID: 15181366.
[31] B. Zifkin and C. Dravet, in *Epilepsy: A comprehensive textbook*, edited by J. Engel and T. A. Pedley (Philadelphia: Lippincott-Raven, 1997).
[32] `https://www.github.com/BrainDynamicsUSYD/nftsim`.
[33] W. J. Firth and A. J. Scroggie, Phys. Rev. Lett. **76**, 1623 (1996).
[34] P. A. Robinson, C. J. Rennie, D. L. Rowe, and S. C. O'Connor, Hum. Brain Mapp. **23**, 53 (2004).
[35] S. Coombes and M. R. Owen, SIAM J. Appl. Dyn. Syst. **3**, 574 (2004).
[36] D. J. Englot *et al.*, Brain **133**, 3764 (2010).
[37] M. Rosanova, O. Gosseries, S. Casarotto, M. Boly, A. G. Casali, M.-A. Bruno, M. Mariotti, P. Boveroux, G. Tononi, S. Laureys, and M. Massimini, Brain **135**, 1308 (2012).
[38] F. H. L. da Silva, W. Blanes, S. N. Kalitzin, J. Parra, P. Suffczynski, and D. N. Velis, IEEE Trans. Biomed. Eng. **50**, 540 (2003).
[39] R. D. Chervin, P. A. Pierce, and B. W. Connors, J. Neurophysiol. **60**, 1695 (1988).
[40] P. Grindrod and D. Pinotsis, Physica D **240**, 13 (2011).
[41] J. Kim, J. Roberts, and P. Robinson, J. Theor. Biol. **257**, 527 (2009).
[42] P. N. Taylor and G. Baier, J. Comput. Neurosci. **31**, 679 (2011).
[43] M. Goodfellow, K. Schindler, and G. Baier, NeuroImage **55**, 920 (2011).
[44] G. Marc, T. P. Neal, W. Yujiang, G. D. James, and B. Gerold, Eur. J. Neurosci. **36**, 2178 (2012).
[45] P. N. Taylor, M. Goodfellow, Y. Wang, and G. Baier, Biol. Cybernetics **107**, 83 (2013).
[46] S. E. Folias and P. C. Bressloff, Phys. Rev. Lett. **95**, 208107 (2005).
[47] S. Coombes and M. R. Owen, Phys. Rev. Lett. **94**, 148102 (2005).
[48] Y. Qi and P. Gong, Phys. Rev. E **92**, 022702 (2015).
[49] P. N. Loxley and P. A. Robinson, Phys. Rev. Lett. **102**, 258701 (2009).
[50] F. Marten, S. Rodrigues, P. Suffczynski, M. P. Richardson, and J. R. Terry, Phys. Rev. E **79**, 021911 (2009).
[51] M. Chen, D. Guo, Y. Xia, and D. Yao, Front. Comput. Neurosci. **11**, 31 (2017).
[52] T. Arakaki, S. Mahon, S. Charpier, A. Leblois, and D. Hansel, J. Neurosci. **36**, 9618 (2016).
[53] M. Chen, D. Guo, T. Wang, W. Jing, Y. Xia, P. Xu, C. Luo, P. A. Valdes-Sosa, and D. Yao, PLoS Comput. Biol. **10**, 1 (2014).
[54] M. Chen, D. Guo, M. Li, T. Ma, S. Wu, J. Ma, Y. Cui, Y. Xia, P. Xu, and D. Yao, PLoS Comput. Biol. **11**, 1 (2015).
[55] T. Proix, V. K. Jirsa, F. Bartolomei, M. Guye, and W. Truccolo, Nat. Commun. **9**, 1088 (2018).